

Spectrometry for urban area remote sensing—Development and analysis of a spectral library from 350 to 2400 nm

Martin Herold*, Dar A. Roberts, Margaret E. Gardner, Philip E. Dennison

Department of Geography, University of California, Santa Barbara, CA 93106, USA

Received 6 August 2003; received in revised form 19 February 2004; accepted 21 February 2004

Abstract

We investigate the spectral complexity and unique spectral characteristics of urban environments using a comprehensive regional field spectral library of more than 4500 individual spectra. Spectral properties of urban surface materials are presented and interpreted, and their separability is systematically analyzed using the Bhattacharyya distance (B-distance) as a quantitative measure of spectral discrimination. We find considerable spectral confusion between urban land cover types (i.e. specific roof and road types) but also show the potential of fine spectral-resolution remote sensing for detailed mapping of urban materials and their condition based on their spectral signal. An evaluation of the most suitable wavelengths for separation of urban land cover identified specific spectral features that provided the best separation. There is a strong indication that current multispectral systems, including IKONOS and LANDSAT ETM+, provide only marginal abilities to resolve these important features and are limited for urban land-cover mapping.

© 2004 Elsevier Inc. All rights reserved.

Keywords: Urban area remote sensing; Spectral library; AVIRIS; Bhattacharyya distance

1. Introduction

The spectral characteristics of urban surfaces are known to be complex. Given the high degree of spatial and spectral heterogeneity of and within various artificial and natural land cover categories, the application of remote-sensing technology to mapping the urban environment requires specific attention to the spectral dimension. Hyperspectral data offer capabilities of improved spectral and spatial urban mapping capabilities (Ben-Dor et al., 2001; Hepner et al., 1998; Roessner et al., 2001). Potential applications related to urban planning and management include mapping impervious surfaces for flood management and urban water quality (Ridd, 1995) roof types for energy use and fire danger (Oke, 1987; Woycheese et al., 1997) and mapping urban transportation infrastructure and quality. For example, impervious surfaces, consisting of roofs, roads, parking lots and other materials impact the urban hydrological system and their flood potential (Ridd, 1995; Schueler, 1994). The presence of roof materials, such as wood shingle, impacts urban fire danger as a potential source of firebrands for spotting (Woycheese et al., 1997). Additionally, the reflec-

tance properties of roofs modify the energy absorbed and thus impact urban energy balance and energy use, and the local climate in the urban boundary layer (Oke, 1987). The condition and age of road surfaces impact the flow of traffic, safety and the cost of maintenance. Improved mapping of road materials and characteristics has the potential of improving current practices in planning, construction and maintaining transportation infrastructure (Herold et al., 2003a).

Since the development of imaging spectrometry in the early 1980s (Goetz et al., 1985), hyperspectral remote sensing has become an important tool for earth observations (Green et al., 1998). The main advantage of hyperspectral remote sensing is the amount of spectral detail it provides. A large number of contiguous bands allow for precise identification of chemical and physical material properties (Goetz et al., 1985). To date, a majority of research has focused on natural targets such as vegetation (e.g. Asner et al., 1998; Roberts et al., 1993; Ustin et al., 1998) and minerals (e.g. Clark, 1999). Far less research has focused on urban areas using hyperspectral data (Ben-Dor et al., 2001; Herold et al., 2003b; Roessner et al., 2001) with few published spectra and limited analysis of their characteristics and separability (see Background section). Several important questions have yet to be answered: What are spectral properties of urban

* Corresponding author. Tel.: +1-805-893-1496.

E-mail address: martin@geog.ucsb.edu (M. Herold).

materials and land cover types? How do those materials differ in their spectral response? What are the important spectral features needed for spectral separation and mapping? In that context, a growing number of studies have begun to employ spectral mixture models to map urban materials at sub-pixel scales (Rashed et al., 2001; Small, 2001a; Wu & Murray, 2003). Their application, however, is limited by the large diversity of impervious materials and a lack of knowledge of their spectral properties. Studies of pure urban spectra, covering a wide variety of materials over a large range of wavelengths with precise spectral sampling (e.g. from regional spectral libraries (material scale)), can aid remote-sensing analysis at the land cover scale. For example, if specific urban materials are not separable within a spectral library, they are unlikely to be spectrally distinct in a remote-sensing dataset.

In this paper, we used a comprehensive field spectral library acquired between 350 and 2400 nm to interpret and analyze their spectral characteristics. The library was acquired in the vicinity of Santa Barbara, CA, in a region consisting of a large diversity of surface types with different geometry, conditions, and age. To categorize the variety of materials and evaluate remote-sensing mapping potential, we applied a hierarchical land cover classification scheme for urban materials and land cover types based on Anderson et al. (1976). The Bhattacharyya distance (B-distance) was applied to assess spectral separability at different classification levels and to determine important spectral features of urban materials. The B-distance also allowed an investigation of most suitable spectral bands for urban classification and mapping.

2. Background

The current state of knowledge about urban materials and their spectral characteristics and separation is inadequate. Driven by recent availability of hyperspectral remote-sensing systems, there has been increasing interest in detailed study of urban spectral properties and their application in remote-sensing-based mapping (Hepner et al., 1998). Investigations of the spectral properties of urban materials have incorporated both laboratory and ground spectrometer measurements as well as airborne and spaceborne remote-sensing instruments. A generally accepted assumption in all related studies is the spectral complexity of urban materials and land cover types (Forster, 1993; Jensen et al., 1983). As a result, research has mainly focused on investigating fundamental issues in spectral properties, behavior and separation of urban targets to provide a more comprehensive knowledge base for applying remote-sensing technology to specific urban mapping applications. For example, Hepner et al. (1998) and Hepner and Chen (2001) compared spectra of different urban land cover types using Airborne Visible Near Infrared Imaging Spectrometer (AVIRIS) data and interpreted their separability

for urban land cover mapping. Ben-Dor et al. (2001) acquired an urban spectral library from 400 to 1100 nm and discussed the importance of different spectral regions for the mapping of urban areas. They argued that the physical and chemical characteristics of different urban surfaces are represented in all parts of the visible (VIS), near infrared (NIR), shortwave infrared (SWIR) and thermal infrared (TIR) spectrum. Analysis of their urban spectral library and Compact Airborne Spectrographic Imager (CASI) data in the VIS–NIR region demonstrated that urban objects have diagnostic fingerprints in this spectral region. Heiden et al. (2001) analyzed urban spectra acquired using HyMap data. They developed a hierarchical thematic classification of urban land cover types and materials and provide preliminary spectroscopic analysis of those targets. A successful application of hyperspectral remote-sensing material mapping in urban areas was presented by Clark et al. (2001). The authors used high-resolution AVIRIS data with continuum-removed spectral feature analysis to derive a detailed map of material/dust accumulations in connection with the World Trade Center attack on September 11, 2001.

Spectra of urban built-up materials show electronic and vibrational absorption features at specific wavelengths resulting from material chemistry. However, specific urban material types may be spectrally similar due to similar material composition, such as asphalt-based roofs and roads, or specific urban materials and bare soil surfaces. Spectral discrimination of these materials is especially difficult at coarse spectral resolution (Mackay & Barr, 2002; Sadler et al., 1991). Another factor adding to urban spectral complexity is urban materials which are commonly non-Lambertian (Meister, 2000). The non-Lambertian behavior of urban materials increases at higher solar zenith angles. While specific targets show forward-scattering behavior (e.g. concrete, aluminum) others tend to be more Lambertian (asphalt or roof tiles) or have a stronger backscattering behavior, especially for increased surface roughness. The Bidirectional Reflectance Distribution Function (BRDF) of these materials is also dependent on the wavelength, and Mackay and Barr (2002) found that some urban materials show better spectral separation at off-nadir viewing geometries. In summary, urban materials are recognized to be spectrally unique and complex (Price, 1998; Small, 2001b), suggesting that they require specific attention for remote-sensing-based land cover mapping.

Although these studies provide important insights into the spectral properties of urban materials, a comprehensive study of urban spectral characteristics, quantitative assessment of spectral separability, and an evaluation of which wavelengths are most suitable for spectral separation is still lacking. The Advanced Spaceborne Thermal Emission and Reflection Radiometer (ASTER) spectral library represents one of the most comprehensive spectral libraries available (ASTER spectral library, 1998). However, the 55 spectra in that library are fairly generic and lack diversity of variable

age, condition and illumination. A more comprehensive spectral library of urban materials is necessary for a more thorough analysis.

All spectral studies must consider the scale of analysis. Laboratory and field spectra commonly consist of a single material illuminated under specific conditions. Airborne and spaceborne observations contain higher within-class variability that is dependent on sensor characteristics. This variability stems from the diversity of materials in the observed area, object geometry, illumination effects, atmospheric interactions, and spectral resolution as well as spectral mixing effects as a function of the spatial sensor resolution (Price, 1997). Spatial resolution determines if the spectral information measured within the Instantaneous Field of View (IFOV) originates from a single land cover object (e.g. a roof) representing a pure material at the specific scale, or if it encompasses multiple objects within the IFOV representing a spectral mixture, e.g. of roof and vegetation. For example, a road surface might consist of different material components (e.g. intimate mixture of minerals) resulting in a spectrally mixed response. Coarse spatial resolution has been commonly cited as a limitation in the use of remote sensing in urban areas (e.g. Hepner et al., 1998; Roessner et al., 2001). In general, a spatial resolution of 5 m or finer is considered necessary for an accurate spatial representation of urban land cover objects (land cover scale) such as building structures or urban vegetation patches (Jensen & Cowen, 1999; Welch, 1982; Woodcock & Strahler, 1987). Field spectra presented in this study are collected at the material scale and represent a single object, although they may include intimate mixtures as described above.

A principal method in spectrometry is the evaluation of the spectral separability between material types and land cover categories, and the selection of a prioritized set of the most suitable bands that contribute the most spectral contrast for the application. Appropriate techniques are available from measures of spectral separability (Chang et al., 1999; Mausel et al., 1990) including the B-distance that has recently been proposed and implemented for related analysis of high-dimensional datasets (Jimenez & Landgrebe, 1999). The B-distance is defined as (Eq. (1)):

$$B = \frac{1}{8} [\mu_1 - \mu_2]^T \left[\frac{\Sigma_1 + \Sigma_2}{2} \right]^{-1} [\mu_1 - \mu_2] + \frac{1}{2} \ln \frac{|\frac{1}{2}[\Sigma_1 + \Sigma_2]|}{\sqrt{|\Sigma_1| |\Sigma_2|}} \quad (1)$$

where μ_i and Σ_i are the mean vector and the covariance matrix of class one and two, respectively. The B-distance was developed to measure the statistical distance between two Gaussian distributions (Kailath, 1967) and incorporates both first-order and second-order statistics, i.e. Eq. (1) is a sum where the first part represents the mean and the second part the covariance difference component (Landgrebe, 2000). In terms of remote sensing, the B-

distance quantifies the spectral separability over the whole spectral range investigated. B-distance analyses have been valued because of the close relationship of this statistical measure to the Bayes-theorem (Hsieh & Landgrebe, 1998) and Maximum Likelihood classification (Bruzzone et al., 1997), and its correlation with the probability of correct classification (Landgrebe, 2000; Mausel et al., 1990). A disadvantage of the B-distance is that it provides no pre-defined thresholds for separability. As a result, only relative separability can be assessed when comparing specific classes or different types of targets at different levels of classification.

3. Methods

3.1. Study area

This study focused on a specific urban region of Santa Barbara and Goleta, CA, USA, located 170 km northwest of Los Angeles in the foothills of the California Coast Range. The land cover types and urban materials found in the area are diverse and make the study site appropriate for the proposed spectral analysis. The AVIRIS image presented in Fig. 1 emphasizes the diversity of land cover types. In addition to the urban cover types, non-urban land cover types include water bodies, green vegetation (usually irrigated urban areas or agriculture), non-photosynthetic vegetation (e.g. senesced grasslands) and bare soil (e.g. constructions sites). The urban area represents different types of land use including residential areas with different densities and socio-economic structure, mixed-use areas, and commercial and industrial districts with various urban built-up cover types such as roofs, roads, parking lots, sidewalks, recreational surfaces and landscaping elements. The urban materials found in these areas result from several decades of development with local and traditional influences, and represent a diversity of material types and conditions comparable to many urban areas in the United States, especially in the southwestern parts (Fig. 1).

3.2. Field library acquisition and processing

Field spectra were acquired with an Analytical Spectral Devices (ASD) Full-Range (FR) spectrometer (Analytical Spectral Devices, Boulder, CO, USA). The FR spectrometer samples a spectral range of 350–2400 nm. The instrument uses three detectors spanning the visible and near infrared (VNIR) and shortwave infrared (SWIR1 and SWIR2), with a spectral sampling interval of 1.4 nm for the VNIR detector and 2.0 nm for the SWIR detectors. All spectra used in this study were resampled to a spectral resolution of 2 nm to create 1075-band spectra. A fiber-optic cable transmits light from the aperture to the spectrometer. Both the bare fiber, with a field of view of 22°,

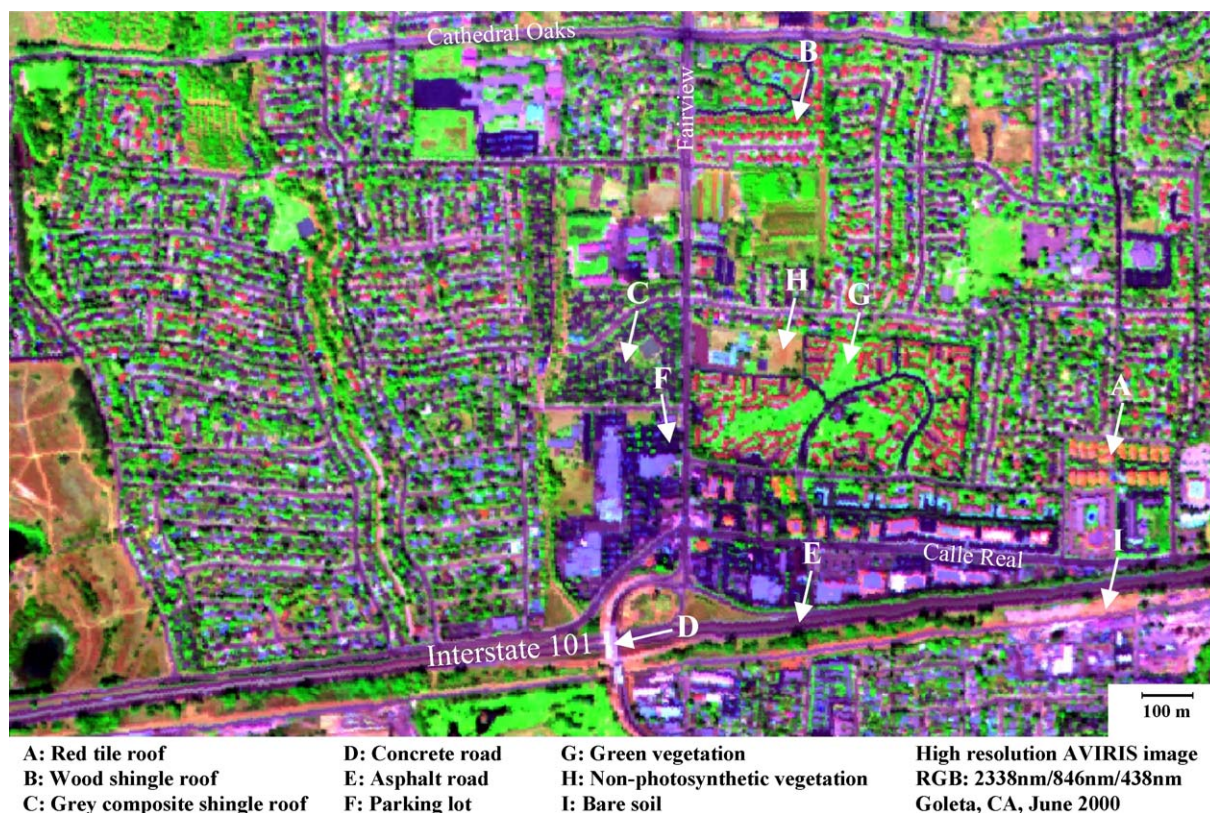


Fig. 1. AVIRIS image of the Fairview study area, Goleta, CA, emphasizing the diversity of materials and land cover types represented in the spectral library.

and an 8° field of view foreoptic lens were used to acquire field spectra. FR field spectrometer data are widely used and considered to provide accurate and high-quality spectral measurements. However, the spectra show some sensor-specific features with small-scale variations between 950 and 1000 nm and at 1795 nm. High-frequency noise between 950 and 1000 nm results from a low signal at the edge of the 934-nm water vapor band and at the long wavelength edge of the VNIR detector. An offset at 1795 nm results from a transition from the SWIR-1 to SWIR-2 detectors for this instrument. In general, the major water absorption bands (1340–1480 and 1770–1970 nm) were excluded from the statistical analysis. Other sensor-induced spectral variations relate to the somewhat “noisy” signal in the SWIR region above 2300 nm, particularly evident in low reflectance targets. These features will adversely impact the statistical analysis by increasing wavelength-specific variance and potentially decreasing separability. However, they are on average less than 1% reflectance, and also located within wavelength regions that are subject to strong water vapor absorption and thus could be suspect when analyzing airborne or spaceborne data.

The spectra of characteristic urban surfaces, including a large variety of roof and road types, were measured in the Santa Barbara urban area between May 23 and June 5, 2001. The majority of measurements were taken within 2 h of solar noon, except a few spectra that were acquired at higher solar zenith angles to study the effect of different Sun

angles. Most surface materials were measured in situ, although spectra of new roofing material were also acquired for several roofing types. Spectra of in situ materials were acquired from a height of 1 m using the bare fiber optic, with a field of view of 22° (1200 cm^2 at a height of 1 m). Spectra of new roofing materials were acquired from a height of 0.15 m, using an 8° foreoptic lens (14 cm^2 at a height of 0.15 m). The urban materials were measured in sets of five spectra for each field target. Four to six sets of spectra were bracketed by measurements from a Spectralon (Labsphere, North Sutton, NH, USA) 100% reflective standard. All spectra were inspected for quality and suspect spectra were discarded. Each urban surface spectrum was divided by its appropriate standard spectrum to calculate reflectance. Approximately 5500 reflectance spectra, representing 147 unique surfaces, make up the Santa Barbara urban spectral library. The set of 147 targets was reduced to 108 to exclude targets that were either relatively rare (i.e. street paint) or did not have a sufficiently high enough number of field measurements to calculate B-distance. The remaining spectra of 108 targets (~ 4500 individual spectra) were convolved to 224 AVIRIS bands (high-resolution AVIRIS sensor configuration for 2000) assuming a Gaussian filter function and using the full width half maximum and band centers provided by Jet Propulsion Laboratory. Convolution was used to reduce data volume, facilitate data analysis and provide results that are applicable to the AVIRIS sensor.

3.3. Urban land cover classification system

The spectral library consists of ~ 4500 individual spectra that are categorized in 108 unique surface types. This surface type categorization is very detailed but has to be transformed from the material scale to land cover classes to focus the analysis and results to the scale used in classifying land cover, e.g. evaluate the separability between roofs and roads considering all spectral library targets of each land cover type. There were four hierarchical land cover classification levels used in this study (Table 1). Forty-six individual classes were aggregated from the spectral library categories following the Anderson et al. (1976) scheme for

levels I and II modified for this study. The level I classes represent main land cover types such as vegetation, built up, or artificial surfaces, water bodies, and non-urban bare surfaces. Level II subdivides the level I classes based on their use, function or other generic characteristics. The non-built-up classes are not the major focus of the analysis and only very broad level II classes were defined for this investigation.

Levels III and IV (user-defined in the Anderson classification system) further divide the functional land cover classes based on their material properties to represent the complexity of the urban spectral library. Level III represents class detail based on material properties for built-up

Table 1
Land cover classification scheme used for the analysis

Level 1	Level 2	Level 3	Level 4	
1. Built up	1.1 Buildings/roofs	1.1.1 Composite shingle roof	1.1.1.1 Black shingle	
			1.1.1.2 Blue shingle	
			1.1.1.3 Brown shingle	
			1.1.1.4 Green shingle	
			1.1.1.5 Grey shingle	
			1.1.1.6 Mixed shingle	
			1.1.1.7 Orange shingle	
			1.1.1.8 Red shingle	
			1.1.1.9 Tan shingle	
			1.1.1.10 White shingle	
		1.1.2 Plastic roofs		
		1.1.3 Glass		1.1.3.1 Light Glass
		1.1.4 Gravel roof		1.1.4.1 Gray gravel
			1.1.4.2 Red gravel	
		1.1.5 Metal roof		1.1.5.1 Brown metal
			1.1.5.2 Light grey metal	
			1.1.5.3 Green metal	
		1.1.6 Asphalt roof		1.1.6.1 Light grey asphalt
		1.1.7 Tile roof		1.1.7.1 Red tile
			1.1.7.2 Gray tile	
	1.1.8 Tar roof		1.1.8.1 Black tar	
		1.1.8.2 Brown tar		
	1.1.9 Wood shingle roof		1.1.9.1 Dark wood shingle	
	1.2 Transportation areas	1.2.1 Asphalt roads	1.2.1.1 Light asphalt (old)	
			1.2.1.2 Dark asphalt (new)	
			1.2.2 Concrete roads	1.2.2.1 Light concrete
			1.2.3 Gravel roads	1.2.3.1 Light Gravel
			1.2.4 Parking lots	1.2.4.1 Dak Parking lot
			1.2.5 Railroad	1.2.5.1 Railroad tracks
			1.2.6 Walkways	1.2.6.1 Light concrete
	1.2.6.1 Red brick			
	1.2.7 Street paint		1.2.7.1 White street marks	
		1.2.7.2 Yellow street marks		
		1.2.7.3 Red street marks		
		1.2.7.4 Blue street marks		
		1.2.7.5 Other street marks		
	1.3 Sport infrastructure	1.3.1 Tennis courts		
		1.3.2 Red Tartan		
		1.3.3 Basketball court		
2. Vegetation	2.1 Green vegetation			
	2.2 Non-photosynthetic vegetation (NPV)			
3. Non-urban bare surfaces	3.1 Bare soil			
	3.2 Beach			
	3.3 Bare Rock			
4. Water bodies	4.1 Natural/quasi-natural water bodies			
	4.2 Swimming Pools			

classes. The further separation in level IV is based on spectral properties in the visible spectrum (color) or more specific material characteristics. The diversity of level III and level IV classes results from many factors such as building types, cost and age of the building structure, and the socioeconomic/urban land use characteristics in that neighborhood.

There are several urban material and surface characteristics that are not reflected in this classification scheme. Examples are materials properties such as grain sizes, specific material compositions (e.g. minerals, oily components), or structural features such as surface roughness. These properties are considered within-class variability, i.e. two asphalt roads containing rocky components from different geologic backgrounds that are reflected in the spectra are still considered part of one land cover class. Another feature that strongly influences the spectral signal from urban surfaces is structure and geometry. Surface structure generally appears at different scales. Surface material roughness represents the micro-scale and affects the BRDF and brightness of the object (Meister, 2000). Meso-scale object geometry and roughness result from three-dimensional roof or building structures and micro-topography affecting the slope and orientation of roads. In terms of remote sensing, this scale would approximately correspond to pixel-by-pixel variation or texture in high-spatial resolution sensors systems ($\sim 1\text{--}5$ m resolution). Macro-scale surface geometry mainly results from terrain structures and will result in radiometric remote-sensing image distortions known as topographic effects, described and investigated in many studies using Landsat TM or similar sensor systems.

3.4. Derivation of spectral separability and most suitable spectral bands

The B-distance offers a powerful approach for spectroscopic analysis of the urban spectral library and was the central method applied in this study. The B-distance provides a score for the spectral separability between each pair of material or cover type of interest based on the mean and covariance of the categories (Eq. (1)). In this study the B-distance was calculated using the full spectral range acquired by the field spectrometer from 350 to 2400 nm. Spectra represent individual urban surface types and the investigation of spectral characteristics and separability provides a generic view of their spectral properties and discrimination, and the most important spectral features for their separability. Although the results represent the material scale, they will be evaluated in the context of urban area remote sensing (land cover scale) to provide general assumptions and implications of this study for related applications.

The B-distance was calculated using the public domain program “MULTISPEC” (Landgrebe & Biehl, 2001). The B-distance calculation considered 108 individual targets

from the spectral library. The outcome provides a separability score between each material type resulting in a 108×108 symmetrical matrix of B-distance values. The individual B-distance scores can be aggregated to create “minimum” and “average” class separability (considering all urban material spectra of any two land cover classes, e.g. roofs versus roads). The average separability reflects the overall discrimination between two land cover classes whereas the minimum separability shows the lowest observed discrimination between materials of these land cover classes. Furthermore, the B-distance values were aggregated to identify the spectral bands and features that contribute the largest amount of spectral contrast between classes. This function is implemented in MULTISPEC considering either the best average or the best minimum separability for each category (Landgrebe & Biehl, 2001). The determination of the top score for best overall separability considers all possible band combinations and provides the maximum average B-distance score and the related set of most suitable wavelengths. The set of bands for best minimum separation is based on the best minimum B-distance value over all classes, respectively. A major limitation is that the maximum number of bands available for each combination is limited by the smallest number of spectra for an individual target. For this reason, targets with only a few spectra (2–6) were discarded from the statistical analysis. Even after reducing the library from 147 to 108 materials, the number of bands used for calculating the best average separation was limited to nine and the best minimum separability was limited to seven.

The investigation of most suitable spectral bands considered not only the top score band combinations but also the frequency that specific bands were selected for spectral separation. This analysis ranked sets of optimal wavelength configurations that only show minor differences in their B-distance scores and represent similar band combinations, e.g. usually only one or two bands differ between adjacently ranked sets of most suitable bands. Accordingly, the study considers a more robust assessment of the most suitable bands based on the top 20 band combinations for best average and minimum separability. The frequency of appearance of each band is considered a score for the importance of a band in the separation of urban material categories. The frequency value can reach a maximum of 20 if it is present in all 20 best average or best minimum separability band combinations.

4. Results

4.1. Spectral signatures of urban materials

The classification scheme described above represents land cover heterogeneity in the urban environment. In this section we show representative examples of spectral signatures from the library for different land cover and material types. Fig. 2 presents the spectra of various categories at different classi-

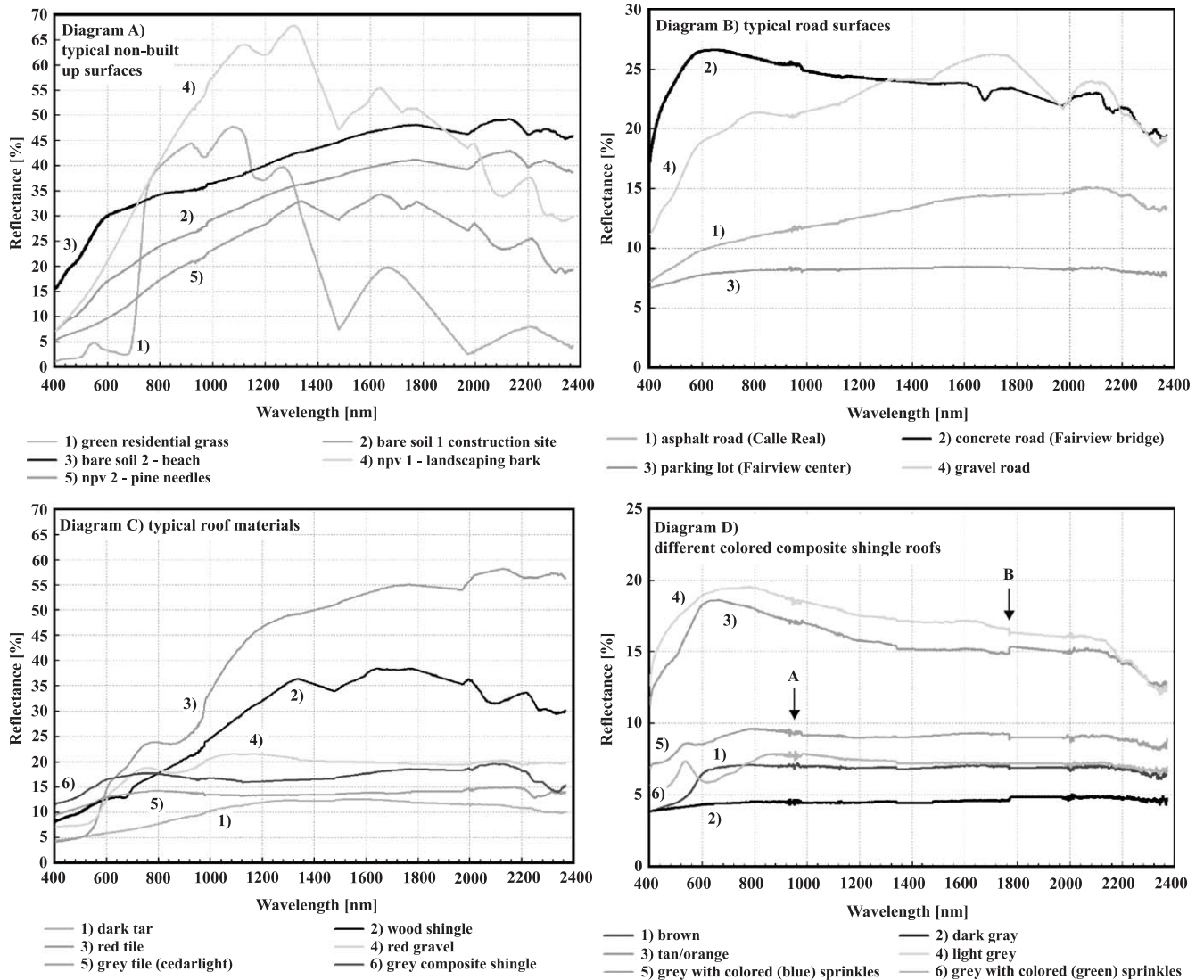


Fig. 2. Spectra of typical land cover types and materials found in urban areas. High-frequency noise present in some spectra between 950 and 1000 nm is due to a low signal near the 934 nm water vapor band and low detector sensitivity at the long wavelength range of the VNIR detector (arrow A in diagram D). A minor peak at 1795 nm represents the transition between the SWIR-1 and SWIR-2 detectors in this instrument (arrow B in Diagram D). Note: different scales are used for each y-axis.

fication levels. Fig. 2-A presents spectral plots of level II non-urban classes. They show the classic spectral characteristics for vegetation with a reflectance peak in green, minima at blue and red due to chlorophyll absorption, high reflectance in the NIR due to internal leaf anatomy and scattering, and decreasing reflectance in the SWIR due to vibrational absorptions by liquid water and leaf components such as lignin and cellulose. The spectra of bare soil show general similarities with the non-photosynthetic vegetation (NPV) targets in visible and near-infrared parts of the spectrum. However, the NPV spectra have significant ligno-cellulose vibrational absorption bands nears 2100 and 2300 nm that clearly identifies them as such (Roberts et al., 1993).

Fig. 2-B and -C represents level III classification spectra of a selection of roof and road materials. The road materials show a general spectral shape of increasing reflectance at

longer wavelengths and a reflectance peak in the SWIR with concrete and gravel roads having the highest reflectance and parking lots having the lowest reflectance over the whole spectral range. Gravel road spectra represent mineral composition and show related absorption features from the silicates at 2200 nm, hydro-carbonates above 2200 nm, and iron oxides in the visible and near-infrared (near 520, 670 and 870 nm). Asphalt roads represent an aggregate of crushed stones and various chemical components of tar or oil and other hydrocarbons. The major mineral components in the aggregate vary but are dominated by SiO₂, CaO and MgO (Robl et al., 1991). The asphalt spectrum has a very low overall reflectance and only minor absorption features appear from silicates at 2200 nm and hydro-carbonates above 2200 nm. Parking lots are fairly pure asphalt/tar surfaces (parking lot sealant) with low constant reflectance and no significant

absorption features due to the absence of dominant mineral components. Concrete road material is comprised of cement, gravel and water and various other ingredients. Significant absorptions appear in the SWIR due to calcium carbonate with a feature at 2300 nm for calcite and at 2370 nm from dolomite. The roof spectra (Fig. 2-C) indicate the distinct spectral signatures of red tile and wood shingle roofs compared to the other roofing materials with both roof types showing a significant reflectance increase in the NIR and SWIR region. The wood shingle signature contains the ligno-cellulose absorptions in the SWIR that are common for all non-photosynthetic vegetation surfaces (see Fig. 2-A). Ligno-cellulose absorption bands are unique to these types of roofs and appear near 2100 and 2300 nm. The reflectance increase towards longer wavelengths of the red clay tile has been related to loss of water in the production firing process (Heiden et al., 2001). Further significant spectral features are the iron-oxide absorption features at 520, 670 and 870 nm. The gravel roof spectrum is somewhat similar to the gravel road spectrum but indicates a different mineral composition with a strong iron-oxide component. Tar, gray tile and composite shingle materials show the lowest reflectance with only minor absorption features in the SWIR. The different spectra in Fig. 2-D compare different color composite shingle roofs as described by level IV of the classification scheme. There is a general difference in target brightness with more silicate/hydrocarbon absorption features in the SWIR with increase reflectance. Specific small-scale spectral features appear in the visible region representing the color of the roof.

The four diagrams in Fig. 2 clearly indicate the within-class variability within each upper level category, e.g. the spectral variation found for roofs, roads or an individual roof material class. This shows the spectral complexity of the urban environment that has to be considered in any

related image analysis. Fig. 2 also indicates the spectral similarity of some of the categories, e.g. the spectra of asphalt roads, parking lots and some roof types (i.e. composite shingle, tar or gray tile) follow a low, fairly constant reflectance with no unique absorption features. Bare soil surfaces also appear to have a similar spectral trend to specific urban targets with increasing reflectance towards longer wavelength.

Some spectra show high-frequency artifacts near water absorption bands and in transition between detectors in the spectrometer (Fig. 2–4). They are obvious in the spectral signatures (see Fig. 2-D arrows A and B) and affect the statistical analyses as they add variance to the spectra. However, these features were generally less than 1% reflectance and significantly smaller than actual spectral differences between materials. Also, the B-distance separability measurements are mainly based on the mean spectral difference given the whole spectral range and these small features have a minor impact on that. In any case, the evaluation of optimal spectral wavelengths has to consider these noisy spectral areas if suitable bands are located within them.

Fig. 3 represents the spectral variation of different transportation materials. Fig. 3-A shows the spectra of different road conditions due to the aging of asphalt and its effect on spectral response. The natural aging of asphalt is caused by reaction with atmospheric oxygen, photochemical reactions with solar radiation, and the influence of heat, and results in three major processes (Bell, 1989): the loss of oily components by volatility or absorption, changes of composition by oxidation, and molecular structuring that produces thixotropic effects (steric hardening). The loss of oily components is relatively short-term; the other two are more long-term processes. The results of these processes are represented in the spectra. New asphalt surfaces have the lowest reflectance

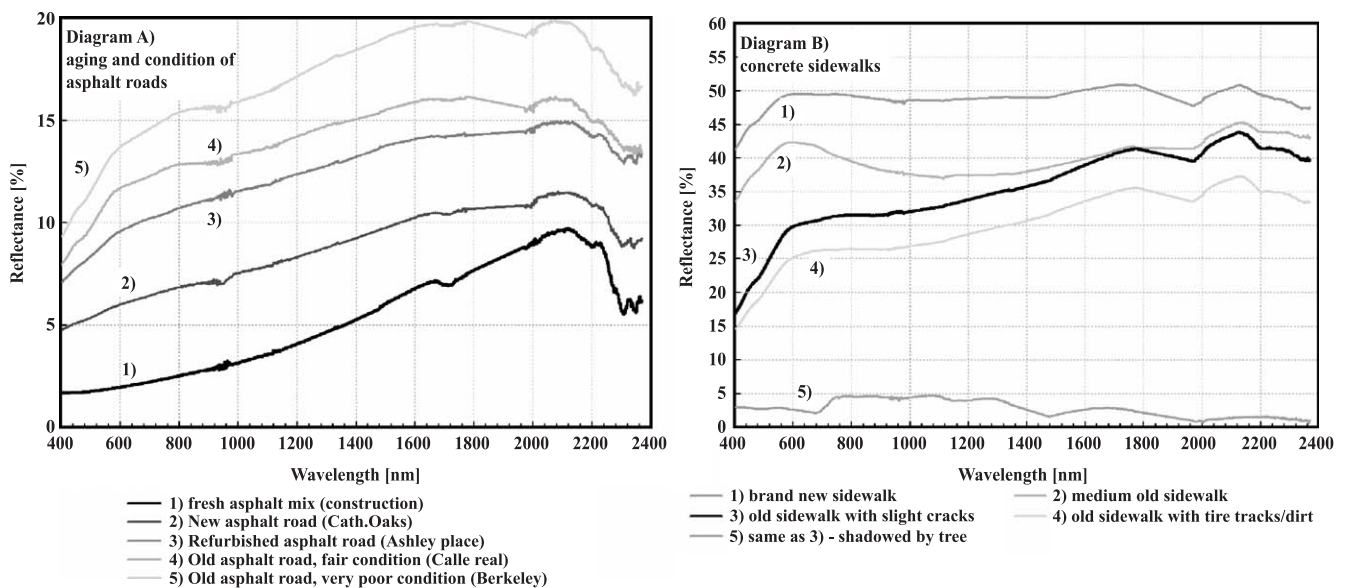


Fig. 3. Spectral representation of asphalt and concrete materials conditions (the major water vapor absorption bands are interpolated; note the different scales in the y-axis).

with an increasing signal towards 2100 nm. As a material ages and its condition deteriorates, reflectance increases in all parts of the spectrum. This observation can be related to the loss of oily components and the sealing tar surface that decreases the general object absorption and the accumulation of dirt and dust on the road surface. The difference in reflectance is highest in the NIR and SWIR, peaking at 14%. The spectral shape in NIR and SWIR changes from convex for new asphalt to concave for older surfaces. The oxidation process is clearly shown by the appearance of iron-oxide absorption features at 520, 670 and 870 nm, especially in spectra 4 and 5 (Fig. 3-A). Other significant small-scale absorption features appear at 2315 and 2350 nm. They represent specific hydro-carbon compounds in the asphalt. Both features are distinct for new asphalt surfaces and vanish with age and poorer surface conditions. For spectra 2–5 the spectral contrast between ~ 2100 and ~ 2350 nm decreases for older asphalt surfaces. In general, the distinct spectral variations that represent the aging and condition of asphalt surfaces represent an interesting spectral contrast that might be used to map road age and specific conditions from hyper-spectral remote-sensing systems (Herold et al., 2004).

Variation in the spectral response from concrete sidewalk surfaces with a change in age or condition is shown in Fig. 3-B. New concrete sidewalk surfaces have the highest reflectance. Material aging and degradation result in a decreased reflectance with the largest reflectance change in the visible and near-infrared region. This change reflects the continued oxidation of the surface shown by increasing iron-oxide absorption features and the accumulation of dust and dirt that decreases the brightness of the concrete surface. The absorption features in the SWIR concrete spectra show minor changes with a clear trend of increasing clay absorp-

tions for older surfaces near 2200 nm. A comparison of the spectral effects of surface age and conditions points out a somewhat contrary development between asphalt and concrete road surfaces. The object brightness increases for asphalt but decreases for concrete and the SWIR absorption features disappear for asphalt but get stronger for concrete roads. This observation should be considered in related analysis of remote-sensing datasets. Spectrum 5 in Fig. 3-B represents a sidewalk surface completely shaded by a tree canopy. The canopy scatters and transmits light downward onto the shaded surface, obscuring the spectral signature of the urban surface and creating a signature that is more characteristic of dark vegetation. While demonstrating overall low reflectance, spectrum 5 (Fig. 3-B) possesses subtle spectral features typical of vegetated land cover, including a red edge, green peak, and water absorption bands. Shadowing is a problem at all resolutions, and spectra containing shadowed land cover should be analyzed with specific attention.

From a remote-sensing point of view, the acquired signal in a pixel results from a mixture of different individual land surface targets. Even in high spatial resolution sensor systems (~ 3 – 5 m spatial resolution) these mixtures can be very heterogeneous within an urban environment. For example, Fig. 4-A shows typical spectra found at or near a road including an asphalt surface, an asphalt bike lane, gravel alongside the road, fresh white street paint and a concrete sidewalk. The asphalt has a comparatively dark spectrum that is significantly different than the other brighter materials. In a mixed road pixel the asphalt should dominate the spectral signal but the bright surrounding materials are high contrast targets and are clearly apparent in remote-sensing observation. An accurate “unmixing” of

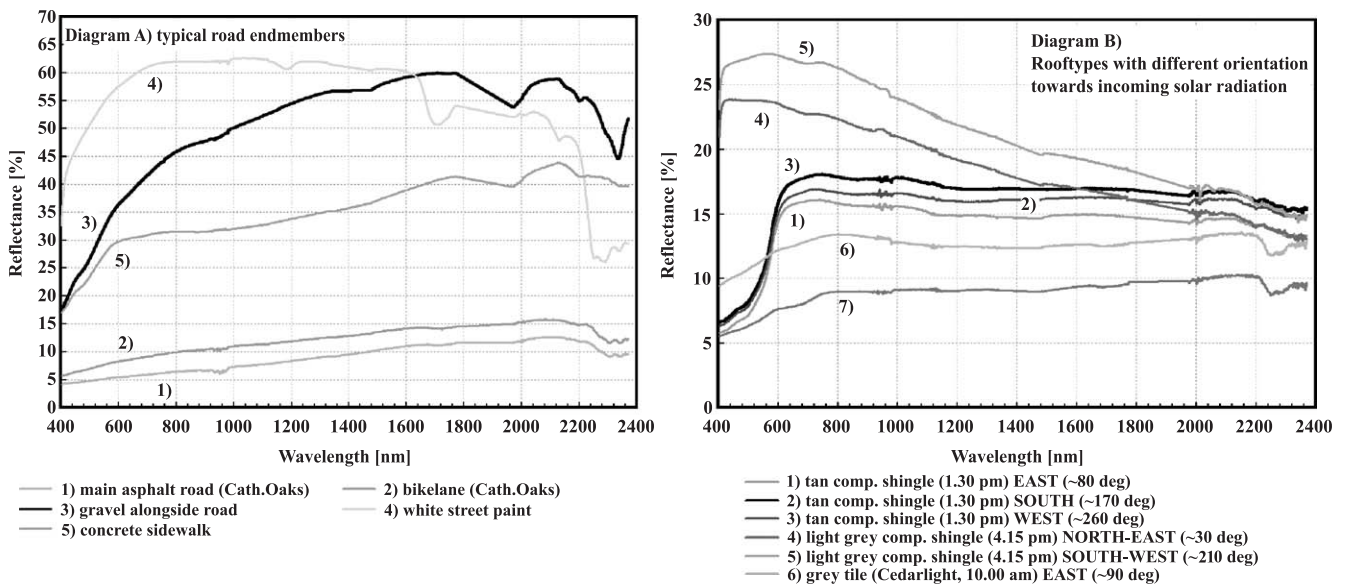


Fig. 4. Spectra of typical road endmembers (left) and the effects of roof orientation on the spectral signatures of roof types (Note: the major water vapor absorption bands are interpolated, the legend for diagram B describes the roof material, the time of spectra acquisition representing the Sun azimuth and the orientation of the roof).

the pixel requires a consideration of all these built-up materials and their relative contributions to the total spectrum. Related analysis requires a comprehensive and sophisticated set of material spectra and appropriate methods for the spectral mixture analysis (Roberts et al., 1998).

The spectral effects of roof geometry, in this case roof orientation, are shown in Fig. 4-B. This plot shows three different types of roofs and their spectral variation at different local zenith angles. For larger Sun angles the brightness of the roof signal decreases with no significant effect on the spectral shape of the roof, at least for the three common roof types shown in this example. However, as shown in previous studies, some urban materials have a strong specular scattering component that changes with wavelength (Mackay & Barr, 2002; Meister, 2000), i.e. some surfaces might show more spectral variations than just brightness effects given changes in solar illumination.

4.2. The spectral separability of urban materials and land cover types

The urban spectral signatures of land cover types and materials found in an urban environment provided some qualitative indication of their separability. A quantitative evaluation of spectral discrimination is provided by the B-distance. The output of the B-distance calculation was a 108×108 symmetric matrix showing the B-distance separability score for each pair of individual spectral library targets. To display the results provided by the 108×108 matrix, we analyzed the B-distance scores on different levels according to the land cover classification system (see Table 1). Fig. 5 shows two diagrams that present the separability scores on classification level I, for built-up and road materials versus major non-built-up classes. Vegetation is represented by both green and non-photosynthetic vegetation, bare land surfaces by bare soil and beach (sand). Each individual point represents a B-distance score between an individual built-up category, specified on the x-axis, and a non-urban class displayed in a specific color. The x-axis shows the library names of the surface material spectra and the level III built-up land cover classes. The continuous lines in the graphs show the mean B-distance value, representing the average separability (geometric mean of the B-distance values) between the built-up target (x-axis) and the specific non-built-up class (color). The number of individual points of a specific color or non-built-up land cover type, respectively, is equal to the number of material spectra of this category used for the analysis. The spread in B-distance of those points indicates the spectral complexity in the land cover type. For example, the class non-photosynthetic vegetation has a relatively large range of B-distance values in Fig. 5. This shows a high within-class spectral variation. The smallest separability scores found for each built-up target show the minimum spectral discrimination and clearly indicate spectral similarities between the specific built-up and non-built-up materials.

The top diagram in Fig. 5 shows an overall high amount of spectral discrimination between roof materials and non-urban targets. Green vegetation (green) and beach surfaces (red) are clearly separable given the mean B-distance scores of about 1000 for most of the roof materials. The mean separability for bare soil (brown) and non-photosynthetic vegetation (NPV, blue) is considerably lower and ranges between 100 and 1000. The roof spectra are most similar to bare soil as it shows the lowest average B-distance values. The smallest separability scores appear for specific NPV targets that have the lowest discrimination with roofs. Some individual values drop below 100 for a few composite shingle roof types and even below 50 for some gray tile roofs and wood shingle roofs.

The spectral discrimination of road materials and major land cover classes is shown in the bottom diagram in Fig. 5. The B-distances have a larger dynamic range than those shown in the upper diagram of non-built-up cover types versus roofs. Similar to roof materials, bare soil (brown) had the lowest average and green vegetation the highest average separability for most of the targets. For asphalt roads, the minimum discrimination scores mainly occurred for bare soil and NPV targets. Concrete roads showed some very low separability values, especially for beach and bare soil surfaces. These peaks indicate some important spectral similarities between these road materials and bright targets of bare surfaces (beach) with the lowest average B-distance values of 30–100. Gravel roads and parking lots showed a better average discrimination. For parking lots, the minimum B-distance scores occur with green vegetation. Those targets represent dark or shaded vegetation surfaces that were spectrally similar to the dark parking lot materials.

The spectral separability between roofs and roads is shown in Fig. 6. This figure corresponds to the level II discrimination in the classification scheme. In terms of average B-distance values, gravel and concrete separate the best for nearly all types of roofs. Parking lots and asphalt roads show a markedly lower average spectral discrimination with dark new asphalt roads and parking lots having the lowest. This is especially true for composite shingle roofs, tar roofs, and gray tile roofs, which had some B-distance minima below values of 50. The smallest individual B-distance values of ~ 10 occurred for dark asphalt roads when compared to composite shingle roofs. These values clearly indicate a low separability for those targets and emphasize that some roof and road materials might not be spectrally distinct enough to be mapped accurately from remote-sensing data. The low minimum B-distance values for concrete roads and some roof types represent an important issue although concrete roads have a comparatively high average separability. This demonstrates that there is a large spectral variability for these surfaces. Low individual discrimination is especially obvious for gravel roofs and gray tile roofs and again represents the general spectral complexity of urban materials. Some land cover types have good average separation while individual targets are spec-

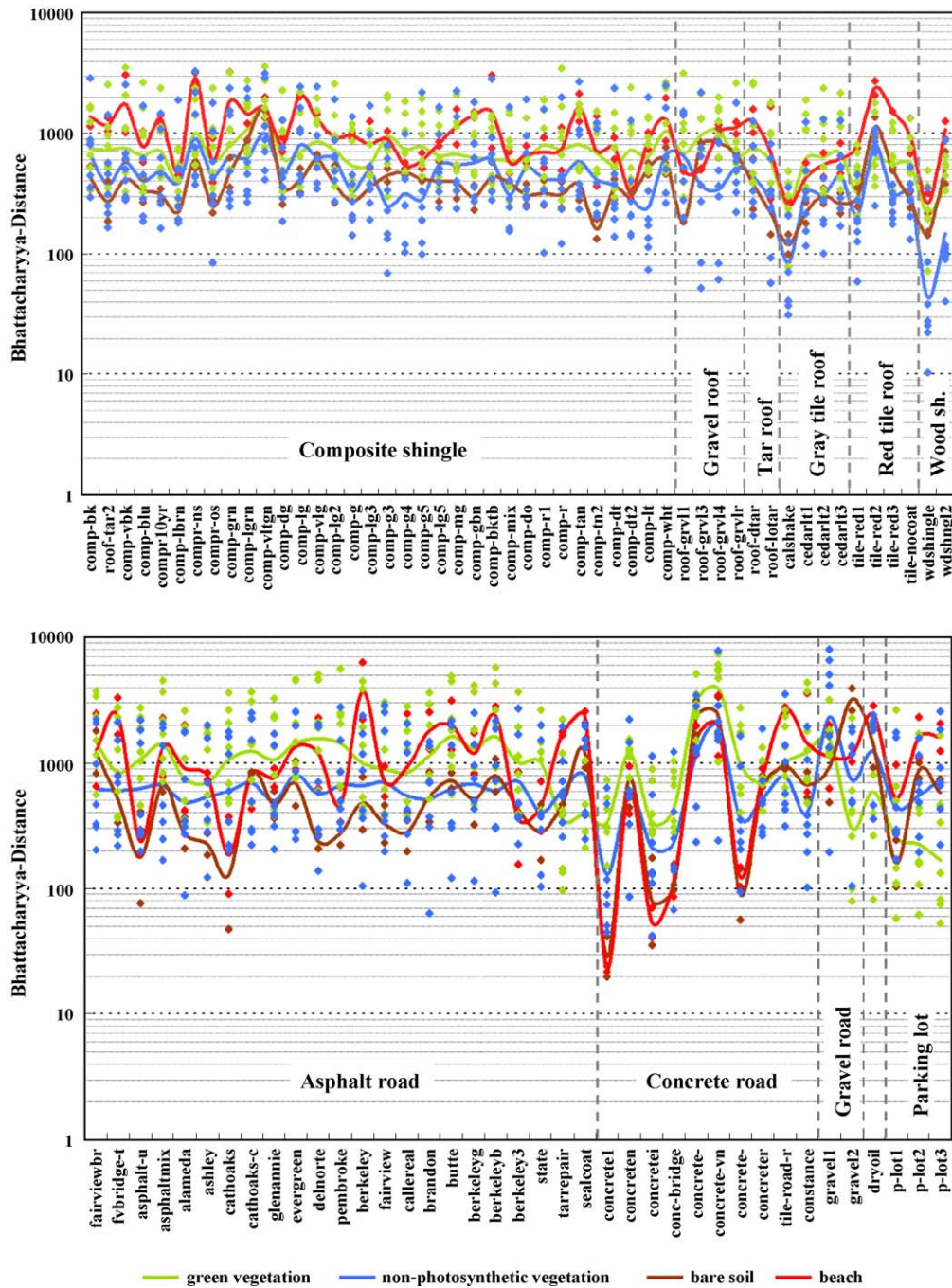


Fig. 5. Spectral separability scores (B-distance) for roof materials (top diagram) and road materials (bottom diagram) versus major non-built-up cover types shown as individual points and average measurements shown as lines (geometric mean, note the logarithmic scale of the y-axis).

trally indistinct compared to other land cover types due to within-class spectral variability.

The average and minimum values of separability for all major urban land cover classes are summarized in Table 2. The results emphasize the generally high degree of separability for green vegetation, gravel roofs, red tile roofs, and roads. Low average and low minimum separability are obvious between asphalt roads, parking lots, and specific types of roof materials such as composite shingle, tar and gray tiles. These classes are spectrally very similar on the

material scale, implying potential difficulty in mapping them using remote sensing. The spectral similarity of these classes has already been observed in their spectral signatures (Fig. 2). These targets are composed of similar materials that generally have related spectral characteristics of nearly constant low reflectance and no significant broad absorption features between 350 and 2400 nm. Their spectral contrast mainly results from differences in brightness that can vary considerably over a wide range of targets (see Fig. 2). Concrete roads have fairly high

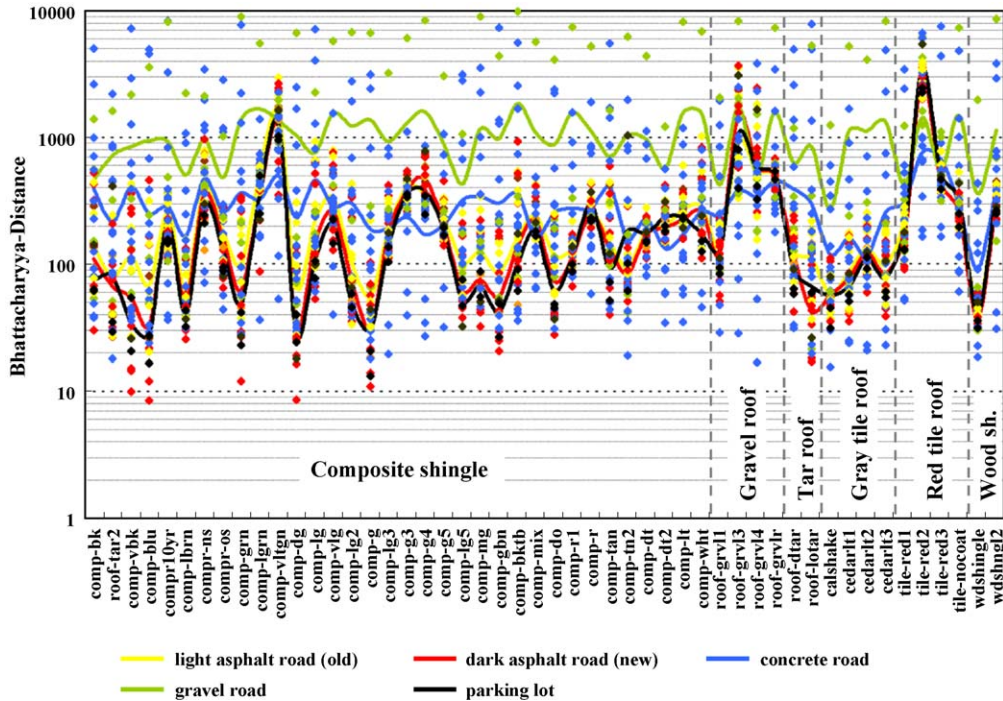


Fig. 6. Spectral separability scores (B-distance) for roof materials versus road materials shown as individual points and average measurements shown as lines (geometric mean, note the logarithmic scale of the y-axis).

average separability scores for all classes. However, their low minimum separability with specific classes such as bare soil, parking lots and several roof types emphasizes a distinct spectral similarity caused by the large heterogeneity of concrete road surfaces.

Wood shingle roofs and NPV represent another pair of classes with good average but low minimum separability. These materials are similar and some confusion between these classes may be observed in remote-sensing data. Gray tile, tar, and composite shingle roofs are confused to a very

high degree. Given the characteristics of remote-sensing observations that theoretically provide a lower spectral separation of urban materials and land cover types, these targets might only be acquired and mapped with insufficient accuracy.

4.3. Most suitable wavelengths in mapping urban areas

The most suitable wavelengths derived from separability analysis of the 108 targets in the spectral library are

Table 2
Average and minimum spectral separability (B-distance) for different land cover types

	1:	2:	3:	4:	5:	6:	7:	8:	9:	10:	11:	12:	13:	14:
	Com_sh	Grav_rf	Tar_rf	Gr_tile	Rd_tile	Wd_sh	Asp_rd	Concr	Grav_rd	P_lot	Gr_veg	NPV	Soil_dk	Soil_be
1: Composite shingle		56	<i>19</i>	<i>14</i>	75	61	<i>8</i>	<i>18</i>	106	<i>13</i>	80	70	133	285
2: Gravel roof	405		<i>36</i>	46	109	189	<i>51</i>	<i>17</i>	88	84	97	52	184	480
3: Tar roof	190	599		<i>30</i>	69	127	<i>17</i>	<i>20</i>	135	<i>26</i>	66	58	145	285
4: Gray tile roof	92	178	67		<i>34</i>	<i>32</i>	<i>35</i>	<i>16</i>	61	<i>31</i>	59	<i>31</i>	99	237
5: Red tile roof	549	581	559	375		84	90	52	147	130	92	59	248	748
6: Wood shingle roof	315	359	171	172	197		218	<i>31</i>	152	249	119	10	378	899
7: Asphalt road	244	693	119	99	1331	351		<i>28</i>	68	<i>7</i>	97	64	48	91
8: Concrete road	687	735	1325	423	1247	977	1151		<i>29</i>	11	59	42	<i>27</i>	20
9: Gravel road	2533	2514	1733	2460	927	4370	3047	1799		117	79	105	485	632
10: Parking lot	194	700	98	81	1499	436	194	897	3832		53	171	104	278
11: Green veg.	992	1066	1023	779	609	426	1614	1589	1106	588		88	64	144
12: Non-photos. veg.	585	646	439	366	511	156	880	887	2288	953	1266		72	84
13: Bare soil (dark)	438	627	330	230	652	542	542	840	2196	801	638	731		218
14: Bare soil (beach)	1152	780	1145	477	1568	1073	1413	1035	1249	1614	889	881	354	

Coding of values: **Bold:** Average separability (lower left part of matrix) / *Italic:* Minimum separability (upper right part of matrix)
Coding of background: Average value ≤ 150 / Minimum value ≤ 20 | 151 ≤ Average value ≤ 300 / 21 ≤ Minimum value ≤ 40

shown in Fig. 7. The graph presents the frequency of each spectral band's appearance considering the top 20 combinations of nine bands for best average separability and of seven bands for best minimum separability. A band can have a maximum frequency of 40 if it appears in all of the top average and minimum channel combinations. In Fig. 7, a fair number of bands have a score of 20 as they appear in all of the top 20 combinations for either best average or minimum separability. For best average separability (shown in black) there are eight; for best minimum separability there are six bands with a score of 20. The rest of the top band appearances are distributed for bands that have a frequency of one since the top-ranked band combinations vary only marginally. Most of these scores appear in a number of adjacent bands (e.g. at 1700 nm) and represent important "most suitable" spectral regions without prioritization of a particular band.

Optimal bands for best average separability appear for nearly all parts of the spectrum. With a frequency of 20, there are several bands in the visible region at 420, 440, 570 and 640 nm, three are in the near infrared at 750, 1105 and 1315 nm and one band in the shortwave infrared at 1990 nm, near a strong water vapor band. Further suitable spectral regions appear for a number of adjacent bands with a frequency of one for seven bands between 490 and 550 nm and nine bands between 1670 and 1750 nm. These spectral regions can also be considered as important for spectral separation.

The distribution of the bands highlights the importance of specific spectral regions. There are five important spectral bands/regions in the visible region showing the contribution of this spectral information. In fact, the color of the urban materials or the absorption features that cause the object color (e.g. iron absorptions) seems to be the most prominent spectral information in separating urban land cover materi-

als. Also, the VIS bands are very close to each other emphasizing small-scale spectral features as important spectral contrast between the targets. There are three more bands/regions in the near infrared and two in the shortwave infrared. These bands represent the consideration of spectral discrimination in this region. They represent the larger dynamic range of reflectance values related to an increase in object brightness towards longer wavelengths for several land cover types (e.g. tile roofs, wood shingle roofs, vegetation, soils, gravel surfaces). There are also specific absorption features for different targets that correspond to the bands of best average separability.

The bands representing the best minimum separability appear with individual bands at 500, 510, 2000, 2010, 2160 and 2330 nm with 19 consecutive bands between 550 and 700 nm. These bands show a more uneven distribution than the ones derived for best average separability. This observation relates to the fact that the minimum value always corresponds to a particular pair of land cover classes that have the lowest separability of all classes. The related most suitable set of bands represents the spectral regions that contribute most to their discrimination. The distribution of the most suitable wavelengths reflects this trend. All of the related bands are located in the visible region and the SWIR and correspond to small-scale absorption features that are important spectral properties of urban materials, e.g. object color or mineral absorption bands. Although these bands are related to the separation of specific classes, they cover different spectral regions than the "best average separability bands" and might have significant contribution to an improved mapping product. The bands near 2000 nm are strongly confirmed by the spectral library data but are located within a CO₂ atmospheric absorption feature. This feature is present in many spectra within the spectral library and thus may be an artifact of a low signal in a strong CO₂

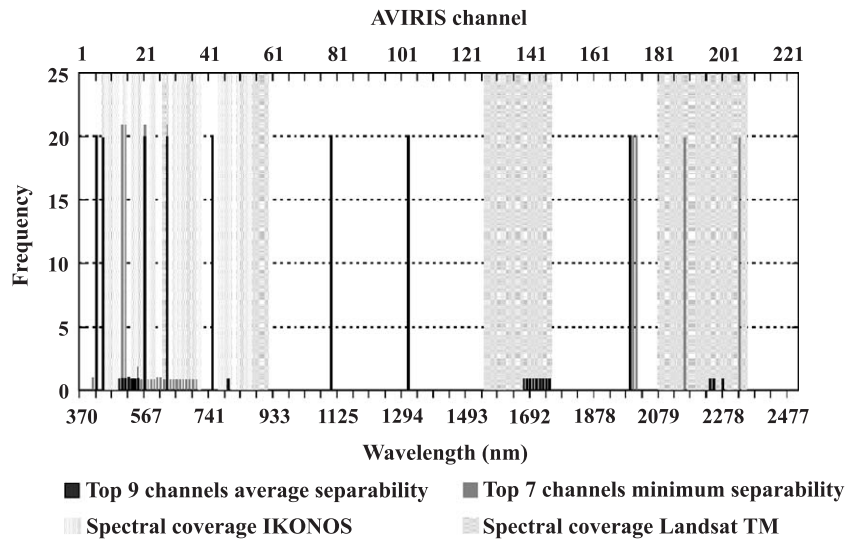


Fig. 7. Frequency of appearance of most suitable spectral bands for best average and minimum separability of 108 targets in the spectral library compared to the spectral coverage of IKONOS and LANDSAT TM satellite sensors.

band. The 1990-nm band, which is at the long-wavelength end of a strong water vapor band, may have a similar problem. Even if they are not artifacts, atmospheric contamination is likely to limit their utility when applied to airborne or spaceborne data.

Fig. 7 also provides a comparison between the locations of most suitable bands and the spectral coverage of two common spaceborne sensor systems, IKONOS and LANDSAT ETM+. This comparison shows that most of the optimal bands lie outside or near the boundaries of the spectral range of those sensors. Furthermore, the broad band character of the channels does not resolve small-scale spectral absorption features especially in the visible and SWIR region that have been described for several built-up and some non-built-up cover types. These results indicate that common multispectral sensor systems only marginally resolve the unique spectral characteristics of many urban materials. Based on this study it is hypothesized that these sensors have significant spectral limitations for mapping the complexity of the urban environment at a detailed level.

5. Conclusions

This study provided a systematic and quantitative investigation of the spectral complexity and unique spectral characteristics of urban environments. A comprehensive regional spectral library of urban materials was developed in the Santa Barbara region. The central method in spectral analysis of the library was the B-distance as a quantitative measurement of spectral separability. This measure was used to assess the discrimination of spectral library targets and evaluate the wavelengths that contribute most to spectral contrast. Although the analysis was accomplished with spectral data that reflect the characteristics of the Santa Barbara urban area, the focus of interpretation and discussion of the results has been on the implications for remote-sensing applications in urban area mapping.

The analysis of spectral separability of urban targets provided a detailed assessment of how specific urban land cover types separate based on their material properties using the B-distance. Some land cover classes are not spectrally distinct over the spectral range between 350 and 2400 nm and have expected limitations in their accurate mapping from remote-sensing datasets. Examples include (a) bare soil targets versus concrete roads; (b) asphalt roads versus composite shingle, tar and gray tile roofs; (c) gray tile roofs versus composite shingle and tar roofs; and (d) asphalt roads versus parking lots. These surface types mainly represent low reflectance targets with no significant broad absorption features. Road surfaces showed the largest variance in their spectral material separability and were especially confused with specific non-transportation cover types. Accordingly, the mapping of transportation infrastructure within an urban environment from remotely

sensed data can be considered as particularly problematic and challenging, at least from the spectral material perspective considered in this study.

The evaluation of most suitable spectral bands clearly represents the spectral diversity of urban environments. The spectral location of the bands emphasizes the important spectral regions that are most useful in separating urban land cover types. The bands highlight the visible region with distinct small-scale spectral variation due to object color. The short-wave infrared bands represent other specific characteristics, absorption features and the brightness increase of many urban land cover types during longer wavelengths. A comparison of the bands most suitable for separating urban targets with the spectral configuration of common multispectral remote-sensing systems showed that the unique urban spectral characteristics are not resolved in those sensors due to the location of the bands and their broadband character, at least considering the results of this study using the B-distance.

There are, however, certain limitations to this study. The spectra had specific noise features that added uncertainty to the statistical analysis. These features are artifacts primarily due to a low signal in the vicinity of strong water vapor absorption bands and at the transition between detectors (950–1000 and 1795 nm). These deviations from the average spectral signal are minor (<1% reflectance) and should not adversely detract from many of the general conclusions of this study. The B-distance approach, because it uses separability scores derived from the full spectral range, also has limitations. There are other techniques that are tailored to specific spectral absorption features that may be more sensitive to subtle spectral differences between materials. For example, one alternative would be to map material chemistry, using fitting approaches such as tetra-corder (Swayze et al., 2003), which has been shown to be capable of mapping very subtle spectral differences in urban materials, such as the presence of trace amounts of asbestiform minerals in the vicinity of the World Trade Center disaster (Clark et al., 2001).

Although this investigation has shown some limitations in separating urban materials and other land cover types the results have also shown great potential in using hyperspectral data in urban area mapping. Detailed investigation into mapping specific roof materials, road types, conditions and aging processes of asphalt surfaces that are of interest should certainly be explored using systems with appropriate sensor characteristics. Previous studies have certainly provided promising results in hyperspectral remote sensing of urban materials (e.g. Clark et al., 2001) and in assessing the effects of spectral sensor resolution in urban land cover mapping accuracy (Herold et al., 2003b). An additional research area for remote sensing of urban landscapes would be to incorporate the spatial dimension in data analysis. The image analysis approaches discussed and explored in this research might help overcome the spectral limitations in mapping urban land cover and help define

necessary spectral characteristics for future remote-sensing systems.

Acknowledgements

The ASD field spectrometer was kindly supplied by the Jet Propulsion Laboratory. The authors would like to acknowledge the support of the U.S. Department of Transportation, Research and Special Programs Administration, OTA #DTRS-00-T-0002 (NCRST-Infrastructure).

References

- Anderson, J. R., Hardy, E. E., Roach, J. T., & Witmer, R. E. (1976). A Land Use and Land Cover Classification Scheme for Use with Remote Sensor Data, U.S. Geological Survey Professional Paper 964.
- Asner, G. P., Wessman, C. A., & Archer, S. (1998). Scale dependence of absorption of photosynthetically active radiation in terrestrial ecosystems. *Ecological Applications*, 8(4), 906–925.
- ASTER spectral library 1998. Available: <http://speclib.jpl.nasa.gov/forms/asp/manmade.htm> (accessed: September 2002).
- Bell, C. A. (1989). Summary Report on the Aging of Asphalt-Aggregate Systems, Strategic Highway Research Program (SHRP) Publications SHRP-A-305, 100 pp., URL: <http://gulliver.trb.org/publications/shrp/SHRP-A-305.pdf> (accessed: September 2002).
- Ben-Dor, E., Levin, N., & Saaroni, H. (2001). A spectral based recognition of the urban environment using the visible and near-infrared spectral region (0.4–1.1 m). A case study over Tel-Aviv. *International Journal of Remote Sensing*, 22(11), 2193–2218.
- Bruzzzone, L., Conese, C., Maselli, F., & Roli, F. (1997). Multisource classification of complex rural areas by statistical and neural-network approaches. *Photogrammetric Engineering and Remote Sensing*, 63(5), 523–533.
- Chang, C. I., Du, Q., Sun, T., & Althouse, M. L. G. (1999). A joint band prioritization and band decorrelation approach to band selection for hyperspectral image classification. *IEEE Transactions on Geoscience and Remote Sensing*, 37(6), 2631–2641.
- Clark, R. N. (1999). Spectroscopy of rocks and minerals and principles of spectroscopy. In A. N. Rencz (Ed.), *Manual of Remote Sensing, Chap. 1* (pp. 3–58). New York: Wiley.
- Clark, R. N., Green, R. O., Swayze, G. A., Meeker, G., Sutley, S., Hoefen, T. M., Livo, K. E., Plumlee, G., Pavri, B., Sarture, C., Wilson, S., Hageman, P., Lamothe, P., Vance, J. S., Boardman, J., Brownfield, I., Gent, C., Morath, L. C., Taggart, J., Theodorakos, P. M., & Adams, M., 2001. Environmental Studies of the World Trade Center area after the September 11, 2001 attack. U. S. Geological Survey, Open File Report OFR-01-0429, <http://speclab.cr.usgs.gov/wtc/> (accessed: February 2004).
- Forster, B. C. (1993). Coefficient of variation as a measure of urban spatial attributes using Spot HRV and Landsat TM data. *International Journal of Remote Sensing*, 14(12), 2403–2409.
- Goetz, A. F. H., Vane, G., Solomon, J. E., & Rock, B. N. (1985). Imaging spectrometry for earth remote sensing. *Science*, 228(4704), 1147–1153.
- Green, R.O., Eastwood, M.L., Sarture, C.M., Chrien, T.G., Aronsson, M., Chippendale, B.J., Faust, J.A., Pavri, B.E., Chovit, C.J., Solis, M., Olah, O., & Williams, O. (1998). Imaging spectroscopy and the airborne Visible/Infrared imaging spectrometer (AVIRIS). *Remote Sensing of the Environment*, 65(3), 227–248.
- Heiden, U., Roessner, S., Segl, K., & Kaufmann, H. (2001). Analysis of spectral signatures of urban surfaces for their area-wide identification using hyperspectral HyMap data. *Proceedings of workshop on remote sensing and data fusion in urban areas, Rome, on CD-ROM*.
- Hepner, G. F., & Chen, J. (2001). Investigation of imaging spectroscopy for discriminating urban land covers and surface materials. *AVIRIS Earth Science and Applications Workshop, Palo Alto, CA* (available: http://popo.jpl.nasa.gov/docs/workshops/01_docs/2001Proceedings.zip (accessed: September 2002)).
- Hepner, G. F., Houshmand, B., Kulikov, I., & Bryant, N. (1998). Investigation of the integration of AVIRIS and IFSAR for urban analysis. *Photogrammetric Engineering and Remote Sensing*, 64(8), 813–820.
- Herold, M., Gardner, M., Noronha, V., & Roberts, D. (2003a). Spectrometry and Hyperspectral Remote Sensing of Urban Road Infrastructure, *Online Journal of Space Communications*, 3, URL:<http://satjournal.tcom.ohio.edu/issue03/applications.html> (accessed: July 2003).
- Herold, M., Gardner, M., & Roberts, D. (2003b). Spectral resolution requirements for mapping urban areas. *IEEE Transactions on Geoscience and Remote Sensing*, 41(9), 1907–1919.
- Herold, M., Roberts, D.A., Smadi, O., Noronha, V. (2004). Road Condition Mapping Using Hyperspectral Remote Sensing, *AVIRIS Earth Science and Applications Workshop*, 31.3 - 2.4.04, Pasadena, CA, available: http://aviris.jpl.nasa.gov/htmlwrkshp_033104.html.
- Hsieh, P. F., & Landgrebe, D. (1998). Classification of High Dimensional Data. Technical Report: TR-ECE 98-4, May 1998, School of Electrical and Computer Engineering Purdue University West Lafayette, URL: <http://www.ece.purdue.edu/~landgreb/Hsieh.TRECE4.pdf> (accessed: September 2002).
- Jensen, J. R., Bryan, M. L., Friedman, S. Z., Henderson, F. M., Holz, R. K., Lindgren, D., Toll, D. L., Welch, R. A., & Wray, J. R. (1983). Urban/suburban land use analysis. In R. N. Colwell (Ed.), *Manual of Remote Sensing, vol II*, Chapter. 30 (2nd ed.) pp. 1571–1661. American Society of Photogrammetry and Remote Sensing Falls Church, VA.
- Jensen, J. R., & Cowen, D. C. (1999). Remote sensing of urban/suburban infrastructure and socio-economic attributes. *Photogrammetric Engineering and Remote Sensing*, 65(5), 611–622.
- Jimenez, L., & Landgrebe, D. A. (1999). Hyperspectral data analysis and supervised feature reduction via projection pursuit. *IEEE Transactions on Geoscience and Remote Sensing*, 37(6), 2653–2667.
- Kailath, T. (1967). The divergence and Bhattacharyya distance measures in signal selection. *IEEE Trans. Communication Theory*, 15, 152–160.
- Landgrebe, D. A. (2000). Information extraction principles and methods for multispectral and hyperspectral image data. In C. H. Chen (Ed.), *Information processing for remote sensing, Chap. 1*. World Scientific Publishing, River Edge, NJ (URL: <http://dynamo.ecn.purdue.edu/~landgreb/publications.html> (accessed: September 2002)).
- Landgrebe, D. A. & Biehl, L. (2001). An introduction to MULTISPEC, URL: <http://www.ece.purdue.edu/~biehl/MultiSpec/2001>, (access: September 2002).
- Mackay, L., & Barr, S. (2002). Assessing the potential of hyperspectral angular imaging of urban built form surfaces for the inference of fine-scale urban land cover information. *Proceedings of 22nd EARSeL Symposium and General Assembly, Prague, Czech Republic*.
- Mausel, P. W., Kramber, W. J., & Lee, J. K. (1990). Optimum band selection for supervised classification of multispectral data. *Photogrammetric Engineering and Remote Sensing*, 56, 55–60.
- Meister, G., 2000. Bidirectional Reflectance of Urban Surfaces, PhD thesis, University of Hamburg, II. Institut für Experimentalphysik, 186 pp., URL: <http://kogs-www.informatik.uni-hamburg.de/PROJECTS/censis/publications.html> (accessed: September 2002).
- Oke, T. (1987). *Boundary layer climates*. New York: Routledge.
- Price, J. C. (1997). Spectral band selection for visible-near infrared remote sensing: spectral-spatial resolution tradeoffs. *IEEE Transactions on Geoscience and Remote Sensing*, 35(5), 1277–1285.
- Price, J. C. (1998). An approach for analysis of reflectance spectra. *Remote Sensing of Environment*, 64, 316–330.
- Rashed, T., Weeks, J. R., Gadalla, M. S., & Hill, A. (2001). Revealing the anatomy of cities through spectral mixture analysis of multispectral imagery: A case study of the greater Cairo region, Egypt. *Geocarto International*, 16(4), 5–16.
- Ridd, M. K. (1995). Exploring a V–I–S (vegetation–impervious surface–

- soil) model for urban ecosystem analysis through remote sensing: comparative anatomy for cities. *International Journal of Remote Sensing*, 16, 2165–2185.
- Roberts, D. A., Gardner, M., Church, R., Ustin, S., Scheer, G., & Green, R. O. (1998). Mapping chaparral in the Santa Monica Mountains using multiple endmember spectral mixture models. *Remote Sensing of Environment*, 65, 267–279.
- Roberts, D. A., Smith, M. O., & Adams, J. B. (1993). Green vegetation, nonphotosynthetic vegetation, and soils in AVIRIS data. *Remote Sensing of Environment*, 44(2-3), 255–269.
- Robl, T. L., Milburn, D., Thomas, G., O'Hara, K., & Haak, A. (1991). The SHRP Materials Reference Library Aggregates: Chemical, Mineralogical, and Sorption Analyses, Strategic Highway Research Program (SHRP) Publications SHRP-A/UIR-91-509, 88 pp., URL: <http://gulliver.trb.org/publications/shrp/SHRP-91-509.pdf> (accessed: September 2002).
- Roessner, S., Segl, K., Heiden, U., & Kaufmann, H. (2001). Automated differentiation of urban surfaces based on airborne hyperspectral imagery. *IEEE Transactions on Geoscience and Remote Sensing*, 39(7), 1525–1532.
- Sadler, G. J., Barnsley, M. J., & Barr, S. L. (1991). Information extraction from remotely sensed images for urban land analysis. *Proceeding of the 2nd European conference on geographical information systems EGIS'91, Brussels, Belgium, April* (pp. 955–964). Utrecht: EGIS Foundation.
- Schueler, T. R. (1994). The importance of imperviousness. *Watershed Protection Techniques*, 1(3), 100–111.
- Small, C. (2001a). Estimation of urban vegetation abundance by spectral mixture analysis. *International Journal of Remote Sensing*, 22(7), 1305–1334.
- Small, C. (2001b). Scaling Properties of Urban Reflectance Spectra, AVIRIS Earth Science and Applications Workshop, 27 Feb–2 Mar 2001, Pasadena, CA., available: http://popo.jpl.nasa.gov/docs/workshops/01_docs/2001Proceedings.zip (accessed: September 2002).
- Swayze, G. A., Clark, R. N., Goetz, A. F. H., Chrien, T. G., & Gorelick, N. S. (2003). Effects of spectrometer band pass, sampling, and signal-to-noise ratio on spectral identification using the Tetracorder algorithm. *Journal of Geophysical Research*, 108(E9), 5105 (doi: 10.1029/2002JE001975).
- Ustin, S. L., Roberts, D. A., Pinzon, J., Jacquemoud, S., Gardner, M., Scheer, G., Castaneda, C. M., & Palacios, A. (1998). Estimating canopy water content of chaparral shrubs using optical methods. *Remote Sensing of Environment*, 65, 280–291.
- Welch, R. (1982). Spatial resolution requirements for urban studies. *International Journal of Remote Sensing*, 3(2), 139–146.
- Woodcock, C. E., & Strahler, A. H. (1987). The factor scale in remote sensing. *Remote Sensing of Environment*, 21, 311–332.
- Woycheese, J. P., Pagni, P. J., & Liepmann, D. (1997). Brand lofting above large-scale fires. *Proc. 2nd international conference on fire research and engineering (ICFRE2), August 3–8, 1997, Gaithersburg, MD* (pp. 137–150).
- Wu, C., & Murray, A. T. (2003). Estimating impervious surface distribution by spectral mixture analysis. *Remote Sensing of Environment*, 84, 493–505.